



# Effect of Disperse Red 1 Azobenzene Dye Doping and Annealing on the Thermomechanical and Photomechanical **Properties of PMMA Fibers**

Zoya Ghorbanishiadeh 🗓, Bojun Zhou 🗓, Morteza Sheibani Karkhaneh 🗓, Rebecca Oehler 🗓 and Mark G. Kuzyk \*

> Department of Physics and Astronomy, Washington State University, Pullman, WA 99164-2814, USA \* Correspondence: kuz@wsu.edu

**Abstract:** This work studies the effect of azobenzene dye Disperse Red 1 (DR1) doping and annealing on the thermomechanical and photomechanical properties of poly(methyl methacrylate) (PMMA) fibers. The mechanical properties are measured as a function of temperature, pump light intensity, and polarization. We find that doping with DR1 increases the stiffness and the glass transition temperature  $(T_g)$  of the PMMA fibers. Moreover, annealing below  $T_g$  decreases Young's modulus and increases  $T_g$ . Finally, the photothermal heating contribution to the photomechanical response and the length change during laser exposure are determined in both unannealed and annealed plain PMMA and DR1-doped PMMA fibers. We find that photothermal heating is the dominant mechanism and the effect of photoisomerization is negligible. The temperature-dependent photomechanical efficiencies are also determined.

Keywords: photomechanics; dye-doped polymers; polymer fibers; photoisomerization; photothermal heating; thermal expansion; anthraquinones; cis and trans isomers; molecular reorientation; angular hole burning; stress; strain

1. Introduction

Poly(methyl methacrylate) (PMMA) is commonly used in fabricating polymer optical fibers (POF). POFs are desirable for their potential in telecommunications applications [1,2], all-optical switches [3–15], light-driven actuators [16], and sensors [11,17]. Environmental factors such as temperature, humidity, and sunlight strongly change the polymer's physical and mechanical properties [18,19]. The operational lifetime of a material depends on interactions with its surroundings. Characterizing their mechanical properties such as Young's modulus under various conditions can be used to model their stability and to determine the proper time for their replacement [19].

Adding dye to the polymer matrix changes its refractive index and enables the fabrication of fiber cores that act as optical waveguides while also imparting a nonlinear optical susceptibility to the material, making it an attractive candidate for fiber-optic-based all-optical device applications [2,20]. These materials also potentially act as light-actuated shape-shifters due to the DR1 dopant, which is an azobenzene dye with two phenyl rings separated by an azo bond (-N=N-) with two isomer states [21]—the elongated trans form and a bent cis form. Upon irradiating with specific wavelengths of light, DR1 undergoes trans-cis and/or cis-trans photoisomerization. The cis-trans transition can also be driven through thermal excitation [16,21–23]. Therefore, the dopants can induce photomechanical effects in the host material through a photothermal change in isomer population or direct photoisomerization, which can be used for photoswitching [21,22]. Heat and light can induce both thermomechanical and photomechanical responses in azobenzene-doped materials that lead to a change in their mechanical properties [16,23]. In contrast, crystals



Citation: Ghorbanishiadeh, Z.; Zhou, B.; Sheibani Karkhaneh, M.; Oehler, R.; Kuzyk, M.G. Effect of Disperse Red 1 Azobenzene Dye Doping and Annealing on the Thermomechanical and Photomechanical Properties of PMMA Fibers. Appl. Sci. 2022, 12, 7991. https://doi.org/10.3390/ app12167991

Academic Editor: Alessandro Pegoretti

Received: 10 July 2022 Accepted: 8 August 2022 Published: 10 August 2022

Publisher's Note: MDPI stays neutral with regard to jurisdictional claims in published maps and institutional affil-



Copyright: © 2022 by the authors. Licensee MDPI, Basel, Switzerland. This article is an open access article distributed under the terms and conditions of the Creative Commons Attribution (CC BY) license (https:// creativecommons.org/licenses/by/ 4.0/).

can have a larger photomechanical response due to their high molecular density [24], but crystals cannot be fabricated into long lengths of optical fiber.

Adding a low-molecular-weight dopant dye to PMMA influences the thermomechanical and photomechanical properties. The addition of dye with sufficient concentration is observed to plasticize the polymer by increasing the free volume of the system [2]. The plasticization decreases the glass transition temperature [25,26] and Young's modulus [2,25,26] of the polymer. However, depending on the conditions, the interaction of dye and host polymer inhibits chain mobility and the free volume while increasing its packing efficiency, which leads to a higher Young's modulus but with lower  $T_g$ . This behavior is known as antiplasticization [2,25–29]. DR1 is a low-molecular-weight molecule; so, it is expected to plasticize the polymer by decreasing its  $T_g$  [30] and stiffness [2]. However, as we will show below, we see evidence of antiplasticization.

Abdel-Wahab et al. studied the mechanical properties of PMMA such as elastic modulus, yield stress, ultimate tensile stress, and strain at fracture at 20–80 °C in 20 °C increments using uniaxial tension and three-point bending tests. They also presented a numerical analysis for identifying the material parameters for elastoplastic and two-layer viscoplasticity constitutive material models. Both tests demonstrated that all parameters were affected by increasing temperature and, at high temperature, (80 °C) PMMA shows superplastic behavior [31].

Amalia et al. demonstrated a method for measuring Young's modulus of materials, including polymers, by processing the image of a bending cantilever beam. To measure the temperature-dependent Young's modulus, they used a controllable oven and estimated the glass transition temperature ( $T_g$ ) of polymer samples by presenting an equation that explains the behavior of the elastic modulus near  $T_g$  [32]. Sorelli et al. studied the mechanical properties of PMMA thin films containing DR1 that are grafted as side-chains in the dark and under illumination with 532 nm-wavelength laser light by nanoindentation experiments. Three experiments were performed to measure and study the viscoelastic properties of the thin film before, during, and after illumination; the creep recovery before and during illumination and constant load; and the transitory behavior of the thin film during indentation under constant load and light modulation. They observed a slight decrease in the elastic modulus, the hardness, and the irreversible viscosity but an increase in the creep coefficient of films upon illumination. They concluded that the transient behavior is related to the population change of the trans and cis isomers in DR1 [33].

In our work, we study the effect of DR1 doping and annealing on the thermome-chanical and photomechanical properties of PMMA fibers. Specifically, we measure the temperature, pump light intensity, and polarization dependence of Young's modulus and stress in both unannealed and annealed plain PMMA and DR1/PMMA fibers. Annealing causes stress and polymer chain alignment to relax and is accompanied by observable changes in the fiber's shape. As such, the annealed samples should be closer to an isotropic state than the unannealed ones. Neat PMMA fiber is used as a control that has no contributions from the presence of a dopant. This allows the contributions of photothermal heating and photoisomerization to the photomechanical response to be isolated. Theoretical models are developed to determine the heating contribution. Coupling the experimental results and the theoretical models isolates the dominant mechanism. Finally, the temperature-dependent photomechanical efficiency of the fibers are determined to assess their promise for device applications. Such work complements studies of the photomechanical response of materials due to photoisomerization and their applications [34–38].

# 2. Theory

# 2.1. The Elastic Model of Photomechanics

Here, we show how the photomechanical response of a material can be characterized by a change in its spring constant and change in equilibrium length upon absorption of light. Other statistical models can be found in the literature [39] that are related to the ones we use here [16,22]. These ideas hold on many length scales from a single molecule to a

Appl. Sci. 2022, 12, 7991 3 of 26

bulk chunk of material. We also show how the important parameters can be determined from a measurement of the force needed to stretch a sample in the presence of light and in the dark.

A tensile test of a solid material relates strain to stress. Our work uses samples in the form of fibers. As such, we measure the uniaxial tensile force resulting when straining a fiber along its axis [40]. The spring constant of the sample is defined as the Force F induced by a change in the fiber's length  $\Delta L$ ,

$$k = \frac{F}{\Delta L}. (1)$$

Young's modulus E, a measure of the stiffness of a material, is a Hookian model in the elastic reversible deformation region. It relates the stress  $\sigma$  to the strain  $\varepsilon$  according to

$$E = -\frac{\sigma}{\varepsilon}.$$
 (2)

 $\sigma$  has units of force per area, and  $\varepsilon$  is the length change per unit length; so, it is dimensionless [16,22,40]. Young's modulus can depend on temperature or intensity of light exposure, a measurement that we later describe.

The fiber drawing process can induce a built-in stress due to polymer chain alignment along the length of the fiber [2]. Annealing can cause the polymer chains to relax to their isotropic state, causing the fiber length and free volume to decrease and curvature to change—an indicator of stress release. As a result, the mechanical properties of an annealed fiber will be different from those of the unannealed ones [2]. The dopant molecules may align with the polymer chains, and only a small degree of alignment has been observed; so, the effect of plasticization appears to be the dominant one affecting the mechanical properties. The effect of molecular orientation is beyond the scope of this paper, but will be the focus of future studies.

# 2.2. Photothermal Heating

This section models the dynamics of light-induced heating and how this effect can be related to the photothermal contribution to the photomechanical effect. In short, light energy is absorbed and converted to heat in the material, which increases the temperature and leads to photothermal expansion. Here, we will consider the force required to keep the length of the fiber fixed for the configuration used in our experiments.

We are interested in two material properties: (1) the stress in the material when the sample length is kept constant as the temperature increases; (2) the response time of the stress as a function of absorbed light intensity. These two properties determine the heating contribution to the photomechanical response [23]. The model described here is based on the work of Ghorbanishiadeh et al. [23].

The rate of temperature increase due to light intensity  $I_0$  that is turned on at time t=0 is given by the heat equation to be [23]

$$\frac{dT}{dt} = -\frac{1}{t_N}(T - T_a) + \frac{I_0 A}{mc},\tag{3}$$

where  $t_N$  is the Newton cooling time constant, T is the elevated temperature due to heating,  $T_a$  is the ambient temperature,  $I_0$  is the absorbed intensity, A is the area of illumination, m is the mass of the illuminated part of the sample, and c is the specific heat. The last term is the heating term.

At infinite time, the temperature increase above ambient temperature is reached when dT/dt = 0; so, Equation (3) gives [23]

$$\Delta T \equiv (T_{\infty} - T_a) = \frac{I_0 A t_N}{mc}.$$
 (4)

Appl. Sci. 2022, 12, 7991 4 of 26

The mass of the illuminated part of the sample can be defined as the illuminated volume v and polymer density  $\rho$  as  $m = \rho v$  [41,42]. Then, Equation (4) becomes [23]

$$\Delta T = \frac{I_0 t_N}{\rho c w},\tag{5}$$

where the volume is given by v = Aw with w being the sample thickness.

Next, we need the temperature-dependent stress to relate the temperature change induced by the light to the photomechanical stress response. As we show later, dye-doped polymers obey the empirically determined function [23]

$$\sigma = \sigma_0 + \frac{\sigma_1}{\left(1 + \left(\frac{T}{T_0}\right)^n\right)}.$$
(6)

Using Equation (6), the linear photomechanical stress response, defined by  $\Delta \sigma / I_0$ , due to photothermal heating is given by [23]

$$\kappa_{\sigma}^{(1)} = -\frac{d\sigma}{dT} \cdot \frac{\Delta T}{I_0}.\tag{7}$$

Using Equations (5) and (6), the photothermal response is given by

$$\kappa_{\sigma}^{(1)} = -\left(-\frac{n(\sigma - \sigma_0)}{T\left(1 + \left(\frac{T_0}{T}\right)^n\right)}\right) \cdot \frac{t_N}{\rho c w'},\tag{8}$$

where  $\sigma_0$  and  $T_0$  will be determined from a fit of Equation (6) to the data.

# 2.3. Photomechanical Efficiency Figure of Merit

Young's modulus and the linear photomechanical response constant can be used to determine the efficiency of transferring mechanical energy to the material from the absorbed light energy. In the configuration where the sample length is constrained to be constant, the photomechanical Figure of Merit (FOM) is given by [16,22,23]

$$FOM = \frac{(\kappa_{\sigma}^{(1)})^2}{E},\tag{9}$$

where  $\kappa_{\sigma}$  is the photomechanical stress response and E is Young's modulus. The FOM can be used to compare materials. The temperature-dependent figure of merit due to the heating mechanism can be determined using the temperature-dependence of Young's modulus and the heating model of the photomechanical response. As will be described later, the temperature-dependent Young's modulus for dye-doped polymers obeys the empirically determined equation [23]

$$E = \frac{E_0}{(1 + (\frac{T}{T_c})^{n'})},\tag{10}$$

where  $E_0$ ,  $T_c$ , and n' are determined from a fit of the data to Equation (10).

The temperature-dependent figure of merit due to the heating mechanism using Equations (8) and (10) is given by [23]

$$FOM(T) = \frac{(\kappa^{(1)}(T))^2}{E(T)} = \frac{\left(\frac{n(\sigma - \sigma_0)}{T\left(1 + \left(\frac{T_0}{T}\right)^n\right)} \cdot \frac{t_1}{\rho cw}\right)^2}{\frac{E_0}{(1 + \left(\frac{T_0}{T}\right)^{n'})}}.$$
(11)

Appl. Sci. 2022, 12, 7991 5 of 26

The figure of merit can be determined either from a direct measurement of  $\kappa^{(1)}(T)$  or E(T). Alternatively, measurements of E(T) and  $\sigma(T)$  at a few temperatures can be used to obtain the parameters  $E_0$ ,  $T_c$ ,  $T_0$ ,  $\sigma_0$ , n, n' from fits of the data to Equations (6) and (10). These parameters, along with knowledge of the heat capacity c, the dimensions and density of the sample, and the response time  $t_1$  of the photomechanical effect for the specific sample, can then be used to evaluate the temperature-dependent figure of merit given by Equation (11). This analytical expression provides the figure of merit for a broad range of temperatures and can be used in material models of the response.

#### 3. Experiment

#### 3.1. Sample Preparation

We study the influence of DR1 on the host polymer by comparing DR1-doped PMMA and plain PMMA fibers. The first step to make a fiber is fabricating preforms. DR1 (purity of 95%) and methyl(metacrylate) (MMA) monomer were purchased from Sigma Aldrich, St. Louis, MO, USA. MMA contains  $\leq$ 30 ppm MEHQ (4-methoxyphenol) inhibitor, which we removed from the monomer solution by passing it through an alumina gravity column.

 $40~\mu L$  Tert-butyl peroxide initiator per 15~mL of MMA is added to the monomer to drive the polymerization reaction and  $40~\mu L$  per 15~mL of MMA of 1-Butanethiol chain transfer agent is added to limit the chain length during the polymerization process. The liquid solution is poured into a test tube and placed in an oven at  $90~^{\circ}C$  for two to three days to fully polymerize the monomer into a solid cylinder. The test tube is shattered to recover the solid polymer cylinder. To make dye-doped polymer, 0.5% DR1 dye by weight is added to the solution. The dye/monomer solution is sonicated until the dye is fully dissolved, and the polymerization process proceeds in the same way as for the undoped materials.

The preform is the resulting cylinder that is formed. It is cut into a rectangular shape, which is then drawn into a fiber with a rectangular cross-section. Plain PMMA fibers are made in the same way, sans dye. The fibers are drawn at a voltage setting of 56–57 V corresponding to the oven temperature of 240 °C and drawing force between 4000 and 8000 dyn [2]. More details on making a preform and fiber drawing process can be found in [2,43]. The polymer fiber tower and preform-making components were all developed at Washington State University, specifically tailored to making polymer optical fibers for telecommunications applications [20]. Figure 1 shows the chemical structures of DR1 trans and cis isomers.

Figure 1. Chemical structures of Disperse Red 1 (DR1) (a) trans isomer and (b) cis isomer.

### 3.2. Apparatus

Figure 2 diagrams the force measurement apparatus. This custom apparatus, similar in principle to the one demonstrated by Harvey and Terentjev [44], was designed and built at Washington Sate University specifically to measure a variety of photorheological properties in materials ranging from stiff dye-doped polymer fibers and thin films to soft elastomers. An inexpensive version [45] of the apparatus was found to give the same results as the more sophisticated one [16]. The 3D translational stage both centers the fiber in the oven and is used to stretch the fiber. A software-controlled stepper motor actuates the translation stage. The sample is mounted between two custom clamps and the upper clamp is attached in series with a force sensor, which connects the translation stage to the clamp. The oven chamber, clamps, and supporting hardware were custom

Appl. Sci. 2022, 12, 7991 6 of 26

made and machined from solid metal. The oven is heated with resistive heating rods and controlled with an Omega Engineering Model CN7800 programmable PID using a k-type thermocouple temperature sensor and interfaced with an Arduino for control and data collection. The stress load cells are inexpensive generic models obtained from Amazon, similar to the SaiDian 0–100 g Load Cell Sensor. The load cell is calibrated as described in the literature [16,45].

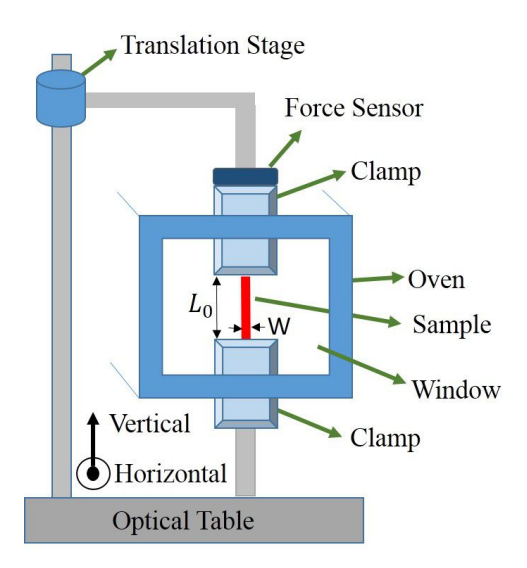


Figure 2. Force measurement chamber.

Young's modulus is determined by translating the translation stage at a constant rate while recording the force sensor reading and the displacement with an Arduino interface as the sample is stretched. Stress versus strain determined from these data and the sample's geometry is fit to a polynomial. The linear part yields Young's modulus of the material, while the tangent gives the stress-dependent Young's modulus. An oven chamber placed around the sample controls the temperature to determine Young's modulus as a function of temperature. These data are fit to the function given by Equation (10).

The temperature-induced stress at constant sample length is determined from the measured stress as a function of temperature while the translation stage is kept stationary. These data are fit to the function given by Equation (6). The parameters determined from these two experiments are inputs to Equation (8).

The load cell measures the force exerted on its ends by the translation stage from above and the sample clamp below. By Newton's third law of action–reaction, each component that is attached in series with the force load cell experiences the same uniaxial force. As such, the stress on each component will result in a strain; so, the displacement of the translation stage will equal the sum of the displacement of all of the components that are in series with it.

The translation stage and clamps are made of massive metal components, which deform negligibly compared with the sample. However, the force sensor is designed to bend, which stretches the electrical wires that are glued to its sides. As such, the deformation of the force sensor must be taken into account.

The contribution of the force sensor's deformation to the displacement of the translation stage is taken into account by assigning it a spring constant K, which is in series with the spring constant k of the sample. The experiment measures the force as a function of displacement, whose ratio yields an effective spring constant  $k_{eff}$  given by

$$k_{eff} = \frac{kK}{k + K'} \tag{12}$$

Appl. Sci. **2022**, 12, 7991 7 of 26

which can be inverted to obtain the spring constant of the sample:

$$k = \frac{k_{eff}}{1 - \frac{k_{eff}}{K}}. (13)$$

Thus, we need to know the spring constant *K* of the force senor to determine the spring constant *k* of the fiber sample.

The spring constant of the force sensor is measured by pushing together the upper and lower clamps in the absence of a sample. In this configuration, the force sensor has by far the lowest spring constant; so, it is responsible for most of the displacement of the stepper motor. The slope of a plot of the force as a function of displacement gives the force sensor's spring constant [16].

After the spring constant is determined for a particular fiber using Equation (13), its Young's modulus is determined from

$$E_{fiber} = \frac{kL_0}{A},\tag{14}$$

where  $L_0$  is the resting length of the part of the fiber between the clamps and A is the cross-section area of the fiber. The spring constant of the fiber in its resting and excited state can be each determined using Equation (13) by performing the measurement without and with illumination, respectively.

Light-induced response measurements require uniform illumination across the entire face of the sample between the mounting clamps. The 488 nm-wavelength krypton/argon laser beam is imaged with a combination of lenses to uniformly illuminate the fiber samples and then to collect the light transmitted through the sample. The resulting force along the vertical axis of the fiber is measured with the force sensor. Figure 3 shows a schematic diagram of the experiment.

Figure 3a shows the configuration used for the polarization-dependent Young's modulus measurements and Figure 3b shows the configuration for polarization-dependent photomechanical stress measurements. The pump polarization is varied between vertical and horizontal for a range of pump intensities. The pump power is in the milliwatt range.

In Figure 3a, the polarizer is used to select the desired polarization axis and the intensity is varied by rotating the half-wave plate. The beam splitter picks off a small portion of the beam to monitor the incident power. The power of the picked-off light and the light transmitted through the sample are measured with a power meter. A cylindrical lens images the beam onto the length of the fiber sample. The transmitted beams are focused onto the power meters with convex lenses to ensure that all of the light is collected. The force is measured as a function of translation stage displacement for a range of intensities for the two orthogonal polarizations at each intensity. These data, when corrected for the effects of the force sensor's elasticity, determine Young's modulus as a function of absorbed light intensity at each pump polarization.

The configuration in Figure 3b is identical to that of Figure 3a, except that the beam splitter is removed and a shutter is added in front of the sample to modulate the pump light. There are two separate experiments as follows:

First, at the start of the experiment while the vertically polarized laser beam is blocked by the shutter, the sample is mounted between the clamps and the data acquisition system is turned on to record the reading of the power meter and the strain. The start of data acquisition is marked as t=0. At t=5 min, the shutter is open to illuminate the sample. At t=20 min, the beam is blocked again and the recording continues until t=25 min. The above protocol is repeated for horizontally polarized pump light. These measurements are used to assess long-term effects on samples under stress and light exposure.

In the second set of experiments, the pump light with fixed polarization and intensity is turned on for 30 s and off for 30 s while the transmitted power and stress are recorded. These provide the step photomechanical response. The intensity is then increased by a

Appl. Sci. 2022, 12, 7991 8 of 26

small increment and the on/off cycle repeated. The intensity is repeatedly incremented to obtain the intensity-dependence of the photomechanical response. The experiment is repeated for pump light of the orthogonal polarization.

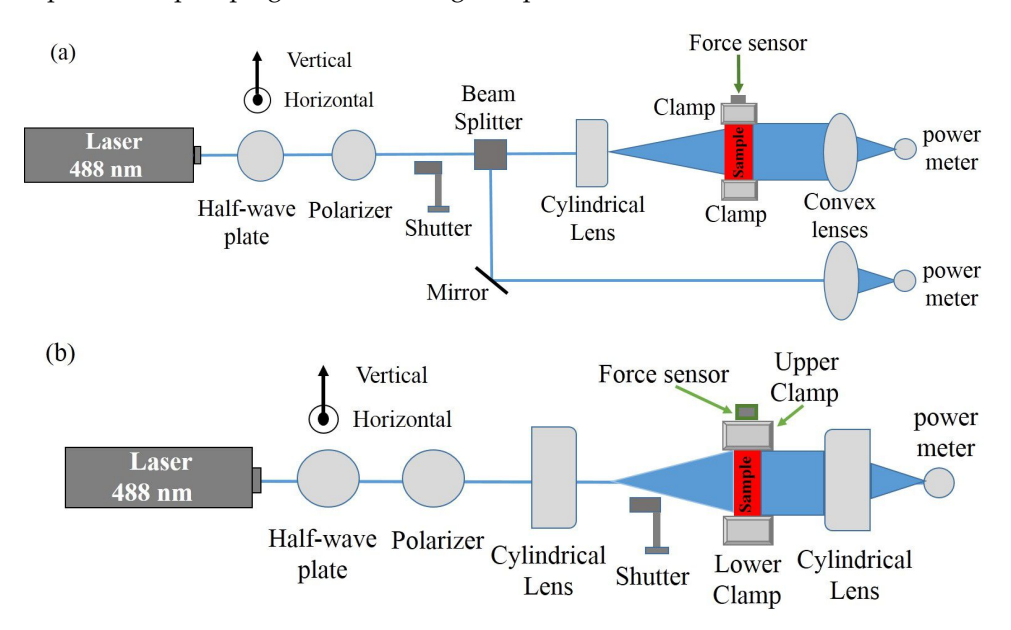


**Figure 3.** The optical path in the experiment to measure (a) Young's modulus as a function of intensity (b) stress as a function of time.

### 3.3. Experimental Procedure

We investigate the effect of annealing on the thermomechanical and photomechanical properties of the fibers by comparing samples that are not annealed with those that are annealed. Each sample fiber is cut into two equal pieces. One of them is annealed in an oven at 90 °C (below the glass transition temperature  $T_g$  [2]) for 5 days. The Young's modulus of the two samples are then measured as a function of temperature in the sample oven chamber in the range of 296.15 to 323.15 K in 3 K increments. The samples soak at each temperature for about 12 min to assure that the fiber is uniformly heated and in thermal equilibrium at the desired temperature. The oven heats the sample from all directions and the small dimensions of the fiber sample ensure that the heat flow is sufficient to reach a uniform temperature profile in far less time than the 12 min provided [46,47]. Then, the sample is stretched at a uniform rate with the stepping motor while the strain is recorded. At the start of each experiment, the sample is slightly prestressed to prevent buckling.

In a second experiment, the temperature-dependent induced stress is measured by recording the stress as the temperature of the oven is increased. Typical temperature ranges are from 293.15 K to 323.15 K over a ramp-up time of 4 min.

The intensity-dependent Young's modulus is measured before, during, and after light irradiation for both vertically and horizontally polarized light at a wavelength of 488 nm. These measurements are repeated for a range of intensities. The light is blocked to measure the elasticity before irradiation. Then, it is measured at different intensities, which are selected by rotating the half-waveplate; finally, the elasticity is measured again when the light is blocked following exposure to the maximum intensity. Moreover, the elasticity is measured at the maximum intensity of both polarizations to double-check the results.

To measure the intensity-dependent stress, the sample is mounted between the clamps and the stress before, during, and after irradiation of vertical and horizontal 488-nm visible light is measured. The duration of illumination is 15 min, followed by 5 min of darkness before and after illumination when the pump beam is blocked. The photomechanical response of a sample is determined for pump light ranging from low to high intensities. The shutter cycles from the off to on state every 30 s to determine the light-induced stress response followed by relaxation of stress.

Appl. Sci. 2022, 12, 7991 9 of 26

The absorbance of visible light by PMMA is negligible. To measure photothermal heating in PMMA, the surface of unannealed and of annealed plain PMMA fibers are painted with a black marker to absorb the light followed by heat transfer to the interior of the fiber [46].

#### 4. Results and Discussion

To study the effect of adding DR1 and annealing on the response of the fibers, a comparison is made between unannealed and annealed plain PMMA and DR1/PMMA fibers. Dimensions and lengths of the samples were measured before and after annealing and showed that there was a small built-in stress in the samples that decreased the length and increased the thickness of the annealed fibers compared with the unannealed ones. Table 1 shows the dimensions of the unannealed and annealed fibers.

**Table 1.** Dimensions and Young's modulus at room temperature of unannealed and annealed PMMA and DR1/PMMA fibers.

Sample	A (mm <sup>2</sup> )	E (GPa)
PMMA-Unannealed	$0.25 \times 0.14$	$2.84\ (\pm0.1)$
PMMA-Annealed	$0.25 \times 0.15$	$2.34 (\pm 0.06)$
DR1/PMMA-Unannealed	$0.25 \times 0.13$	$3.23 (\pm 0.1)$
DR1/PMMA-Annealed	$0.25 \times 0.14$	$2.92 (\pm 0.09)$

# 4.1. Temperature-Dependent Measurements

At the beginning, Young's modulus (E) of unannealed and annealed PMMA and DR1/PMMA fibers is measured at room temperature. The results in Table 1 show that Young's modulus *E* in DR1/PMMA fibers is greater than in PMMA fibers and is lower in annealed fibers compared with the unannealed ones.

Young's modulus as a function of temperature determines the effect of heating and population changes on the stiffness of the samples. Samples are heated from 296.15 °K to 323.15 K in 3 K increments and their elasticity is measured. Figure 4 shows Young's modulus as a function of temperature for unannealed and annealed plain PMMA and DR1/PMMA fibers. The graphs are fitted to the Equation (10), where  $E_0$ , T,  $T_c$ , and n' are Young's modulus at T=0, the oven temperature, the characteristic temperature, and the critical exponent, respectively. Table 2 summarizes the results of the parameters of the fitting function.

Figure 4 shows that increasing temperature decreases the elasticity of the samples and DR1/PMMA fibers have larger elasticity than plain PMMA fibers. Moreover, annealed fibers show lower Young's modulus compared with the unannealed ones.

The glass transition temperature  $T_g$  of the fiber material is measured using differential scanning calorimetry (DSC) with a scanning rate of 10 °C/min. The DSC unit is manufactured by Mettler Toledo and has a temperature accuracy of  $\pm 0.2$  K and precision of  $\pm 0.02$  K based on metal standards. The samples' masses are between 2 and 3 mg. The results show that adding DR1 decreases  $T_g$ . Moreover, annealing the samples increases their  $T_g$ . This is consistent with the results of the characteristic temperature  $T_c$  that is derived using the fitting function, which shows that  $T_c$  in annealed PMMA and DR1/PMMA is greater than in unannealed ones. However,  $T_c$  is unchanged between plain PMMA and DR1/PMMA fibers, implying that adding DR1 did not affect the characteristic temperature.  $T_c$  values of the unannealed fibers are the same within experimental uncertainties, as are the annealed ones. Figure 5 shows the derivative of the heating flow as determined from DSC measurements used to determine  $T_g$ .

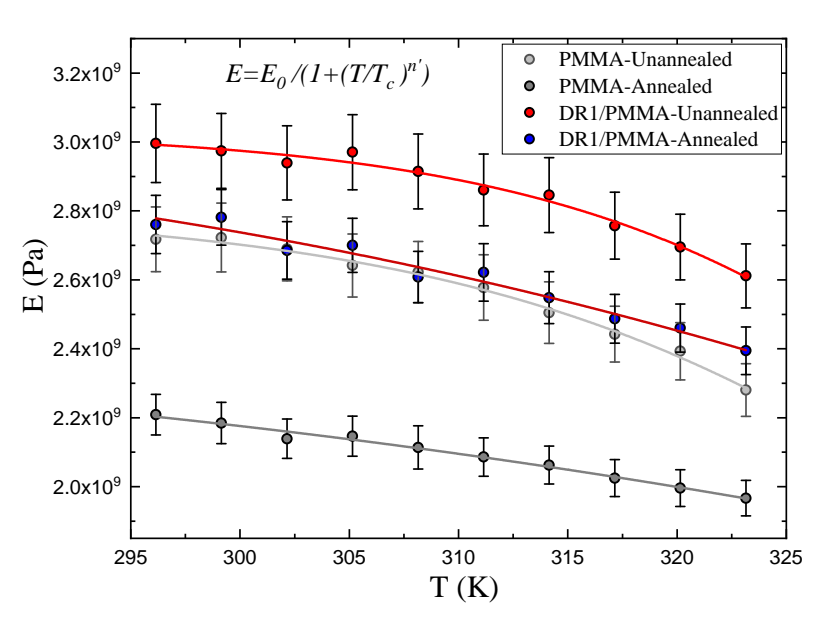


**Figure 4.** Young's modulus as a function of temperature for unannealed and annealed PMMA and DR1/PMMA fibers.

**Table 2.** Parameters of Young's modulus as a function of temperature fitting function for unannealed and annealed PMMA and DR1/PMMA fibers.

Sample	E <sub>0</sub> (GPa)	$T_c$ (K)	n'
PMMA-Unannealed	$2.80 (\pm 0.03)$	$343.56 (\pm 1.81)$	$24.29 \ (\pm 2.54)$
PMMA-Annealed	$2.45 (\pm 0.14)$	$377.26 (\pm 8.99)$	$9.09 (\pm 3.19)$
DR1/PMMA-Unannealed	$3.03 (\pm 0.03)$	$344.23 \ (\pm 2.93)$	$28.79 (\pm 4.17)$
DR1/PMMA-Annealed	$3.06 (\pm 0.25)$	$361.35 (\pm 8.42)$	$11.43 \ (\pm 5.39)$

Table 3 shows the correlations between various combinations of samples using the data in Table 2. The first row shows that there is a significant difference between annealed and unannealed PMMA polymer, as determined from the parameter  $E_0$ —the low temperature limit of Young's modulus, and  $T_c$ —the critical temperature parameter. The difference is not as dramatic for DR1/PMMA. However, adding dye to PMMA has a statistically significant effect on increasing the parameter  $E_0$ . The effect of annealing and dye doping on critical temperature is less obvious, partially due to the fact that the uncertainties are large in the critical exponent n', which affects the accuracy in the determination of  $T_c$ .

**Table 3.** T-test results (and confidence levels) for  $E_0$  and  $T_c$  from Table 2.

Correlations	$t_{E_0}$ (Confidence)	$t_{T_c}$ (Confidence)
PMMA Annealed vs. Unannealed	2.50 (0.9876)	3.67 (0.9998)
DR1/PMMA Annealed vs. Unannealed	0.119 (0.0947)	1.92 (0.9451)
PMMA vs. DR1/PMMA, Both Unannealed	5.42 (0.99999994)	0.194 (0.1538)
PMMA vs. DR1/PMMA, Both Annealed	2.13 (0.9668)	1.29 (0.8029)

In summary, Young's modulus at room temperature results

$$E^{\text{Annealed PMMA}} < E^{\text{Unannealed PMMA}} \le E^{\text{Annealed DR1}} < E^{\text{Unannealed DR1}}.$$

The temperature-dependent Young's modulus of the unannealed fibers are given by

Appl. Sci. 2022, 12, 7991 11 of 26

and

$$T_c^{\text{Unannealed PMMA}} = T_c^{\text{Unannealed DR1}}$$

The annealed fibers give

$$E^{\text{Annealed PMMA}} < E^{\text{Annealed DR1}}$$

and

$$T_c^{\text{Annealed PMMA}} = T_c^{\text{Annealed DR1}}$$

We observe that adding DR1 to PMMA decreases the glass transition temperature  $T_g$ , while Young's modulus E increases. Annealed samples have a measured  $T_g$  in DR1/PMMA fiber that is lower than annealed PMMA fiber, while its E is greater. Moreover, in both fibers, annealing increases  $T_g$  and decreases E.

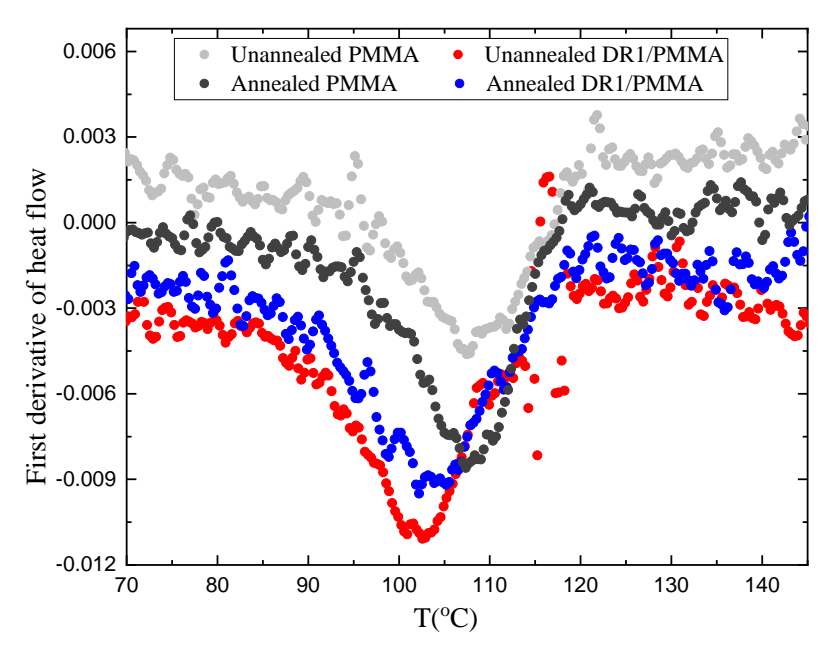


**Figure 5.** First derivative of heat flow from differential scanning calorimeter measurements of unannealed and annealed PMMA and DR1/PMMA fibers used to estimate the glass transition.

Adding DR1 to PMMA is expected to decrease its  $T_g$  due to DR1's plasticizing effect on PMMA [30] and to reduce the stiffness of the polymer compared with the plain PMMA fibers. However, these fibers show that while  $T_g$  in DR1-doped samples decreases, their E increases. This phenomenon is known as antiplasticization [2,25–29]. Here, it is observed that DR1 molecules can induce an antiplasticization effect that can decreases the mobility of the chains and their free volume and increases the packing efficiency of the sample, which increases the modulus [2,25–29]. Moreover, annealing decreases polymer chain alignment, which reduces their stiffness and increases their entropy [2]. This process decreases the free volume, thus, yielding a higher  $T_g$  compared with unannealed fibers.

Stress as a function of temperature is measured for unannealed and preannealed DR1-doped and undoped PMMA fibers. The results for the samples that are heated from 293.15 K to 323.15 K over 4 min are shown in Figure 6. Stress as a function of temperature data is fit to the function

$$\sigma = \sigma_0 + \frac{\sigma_1}{(1 + (\frac{T}{T_0})^n)},\tag{15}$$

where *T* is the sample temperature and the fit parameters are  $\sigma_0$ ,  $\sigma_1$ ,  $T_0$ , and n.

These parameters have physical meaning.  $\sigma_1$  is the temperature-dependent stress contribution in the limit of zero temperature while  $\sigma_0$  is a stress offset due to the stress applied by the clamps when the sample is mounted.  $T_0$  is the temperature at which the temperature-dependent stress falls to half its value. n is an exponent that quantifies the rate at which the stress changes as a function of temperature at  $T_0$ . For samples that have multiple phase transitions, the stress would be a sum over expressions of the form given by Equation (15)—one for each phase transition. The stress for the temperature range in the present studies is described well by a single transition.

The analytical form of Equation (15) with the fitting parameters determined from a fit to the data is used to determine  $d\sigma/dT$  for each fiber for a range of temperatures. Using an analytical fit function provides a cleaner determination of the derivative than would the raw data. The derivative  $d\sigma/dT$  is related to the thermal expansion coefficient. As the fiber is slightly stretched when mounted to prevent buckling when its length increases, an expanding fiber will result in a decrease of the stress; so,  $d\sigma/dT < 0$ . This can be understood from the fact that the fiber's resting length is less than its stretched length at the start of the experiment. If the fiber's resting length increases due to light actuation, the force read by the sensor decreases as the resting length grows closer to the stretched length, which is fixed by the distance between the clamps.

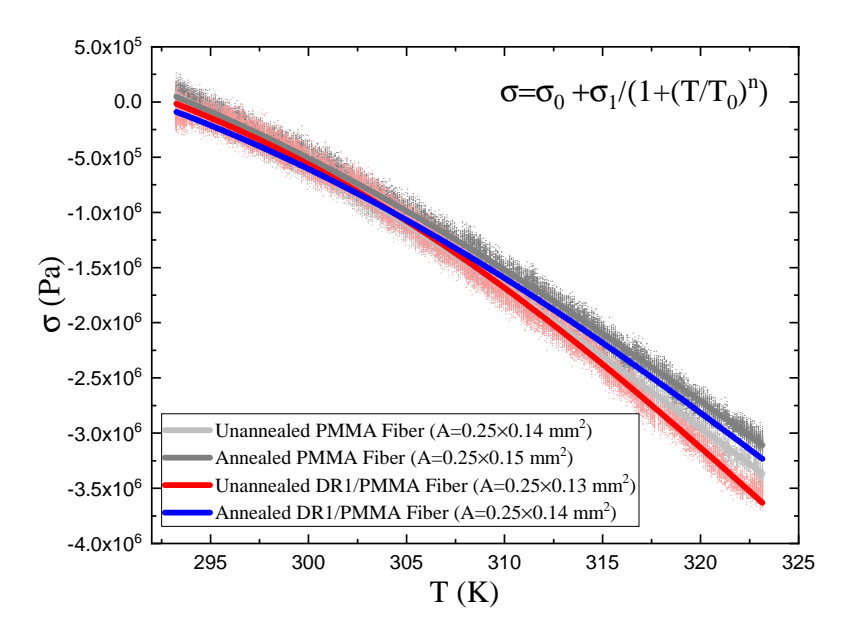


**Figure 6.** Change in stress of a stretched fiber as a function of temperature for PMMA and DR1/PMMA fibers. Note that the fiber is slightly stretched between the clamps to prevent buckling; thus, when the fiber expands, the stress decreases as the stretching strain decreases.  $\sigma_0$  is an arbitrary offset due to the nonzero reading of the sensor when no stress is applied.

Figure 7 shows that all dye-doped fibers have a positive thermal expansion coefficient. For temperatures above 308.15 K, the temperature-induced stress change is larger for unannealed DR1/PMMA fibers than for annealed ones. Similarly, the stress derivative  $d\sigma/dT$  in annealed plain PMMA fiber is lower than in the unannealed ones. So, annealing is observed to decrease the thermal expansion coefficient. Finally, dye-doped fibers show greater thermal expansion than plain fiber, an effect that is most pronounced at the highest temperatures.

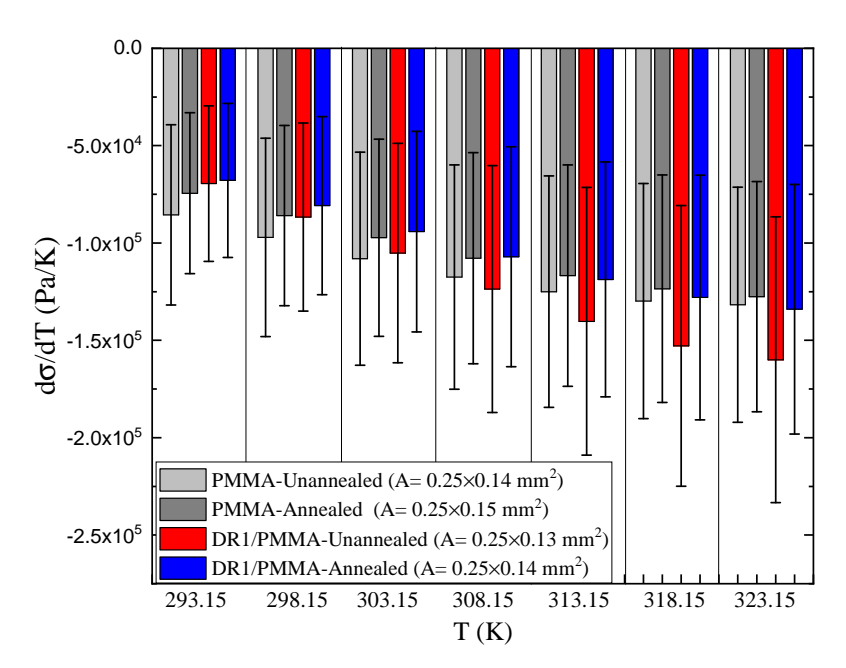


**Figure 7.** The stress derivative as a function of temperature for PMMA and DR1/PMMA fibers that are unannealed and annealed.

To understand the results, we consider two processes that lead to thermal expansion. First, the polymer expands as the temperature increases due to the polymer chains getting excited with thermal energy. Secondly, a change in temperature affects the relative populations of the two isomers of the dopant molecules [16,23]. The competition between these two processes determines the net response. Figure 7 shows that the thermal expansion coefficient of the dyedoped fibers grows relative to the undoped fibers with temperature. The dye dopant appears to enhance the thermal expansion coefficient. The cis isomer population increases at higher temperatures and, given its larger volume, adds to thermal expansion in the DR1/PMMA fibers. The glass transition temperature  $T_g$  is lower in DR1-doped fibers than in plain ones. Since the thermal expansion coefficient increases as the temperature is increased, the larger stress change in DR1/PMMA relative to plain PMMA at a fixed temperature might be explained by this depression in the glass transition in doped polymers. Moreover, annealing the samples increased their  $T_g$  by decreasing their free volume; so, the rearrangement of molecules in the annealed samples is smaller than the unannealed ones, leading to a smaller thermal expansion coefficient in the annealed samples.

# **Intensity-Dependent Measurements**

Here, we characterize the mechanical properties of fibers that are exposed to 488 nm-wavelength light produced by a krypton/argon laser as a function of intensity and polarization. Young's modulus is measured before, during, and after irradiation to determine the immediate and persistent effects of the light. Figures 8 and 9 show typical stress–strain curve data for unannealed PMMA and DR1/PMMA fibers illuminated with vertical and horizontal pump light polarizations.

The flat part in Figures 8 and 9 is due to mechanical backlash in the mounts and is excluded when determining Young's modulus. The stress is observed to decrease during irradiation and persists to varying degrees in both PMMA and DR1/PMMA fibers after irradiation at the maximum intensity. In plain PMMA, the horizontally polarized pump has a larger influence on the stress change than the vertically polarized pump. In both cases, the stress persists when the pump is turned off at the same level as when the pump is on at its maximum intensity.

In dye-doped fiber, the horizontal pump also has the largest influence on the stress change. However, the level of persistent stress after the pump is turned off is less than at its maximum value when the pump is on. These observations imply that the DR1 dopant

contributes to the stress change in the presence of light but that its contribution is reversible, while that of PMMA is not. Since these are unannealed samples, the irreversible part of the stress change is most likely due to a light-induced relaxation of the polymer chains, perhaps from photothermal heating.

To observe the process directly in real-time, the light-induced stress at fixed strain is measured as a function of time as the fibers are irradiated with the maximum light intensity in the mW range for 15 min for both horizontal and vertical pump polarizations. Figure 10 shows the stress as a function of time for unannealed PMMA and DR1/PMMA fibers for 5 min with the pump off, 15 min with the pump on, then 5 min with the pump off. A slight monotonic decrease in stress over time is observed for unannealed PMMA. Upon illumination with 488-nm light, the stress in the DR1/PMMA fiber decreases by about 0.4 MPa. Blocking the pump light after 15 min returns the stress to a level about 0.1 MPa below the starting value. The behavior is the same for both polarizations and for unannealed and annealed fibers.

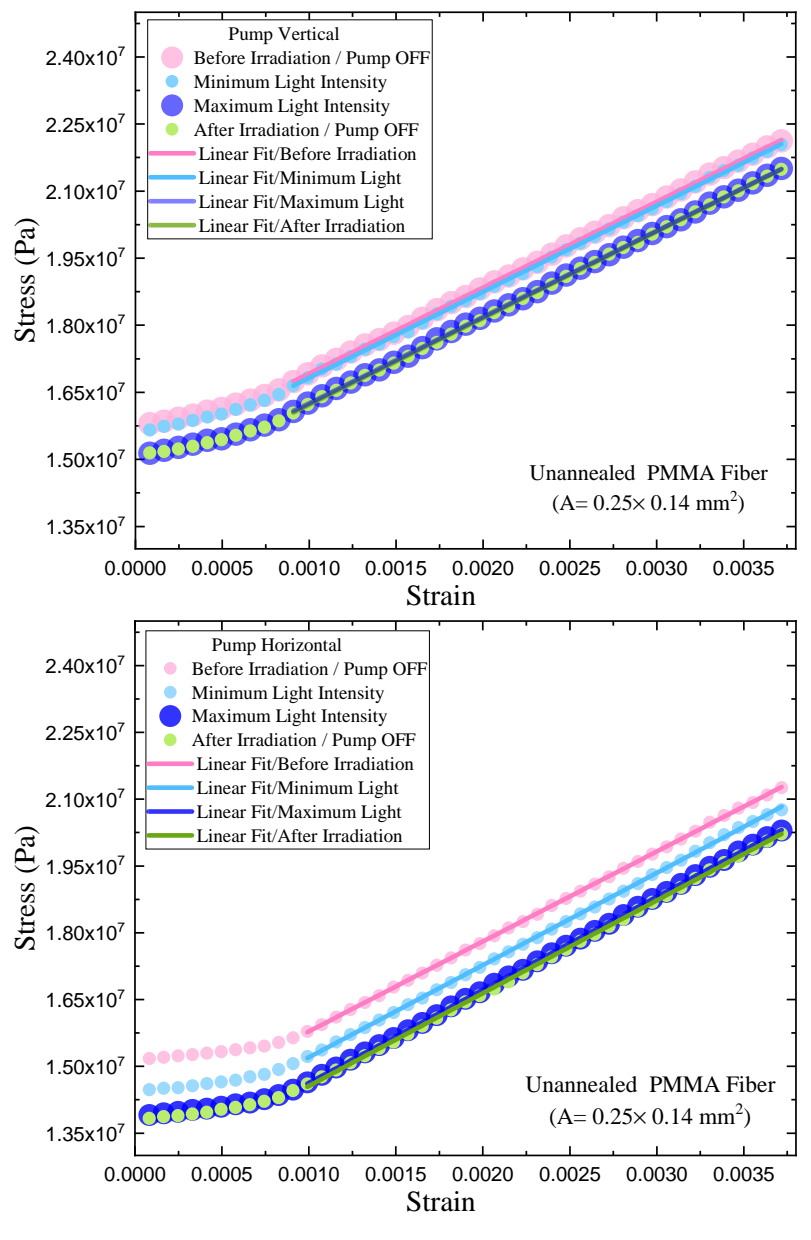


**Figure 8.** Stress versus Strain of unannealed PMMA fiber before, during, and after visible light irradiation with vertical and horizontal polarization.

Appl. Sci. 2022, 12, 7991 15 of 26

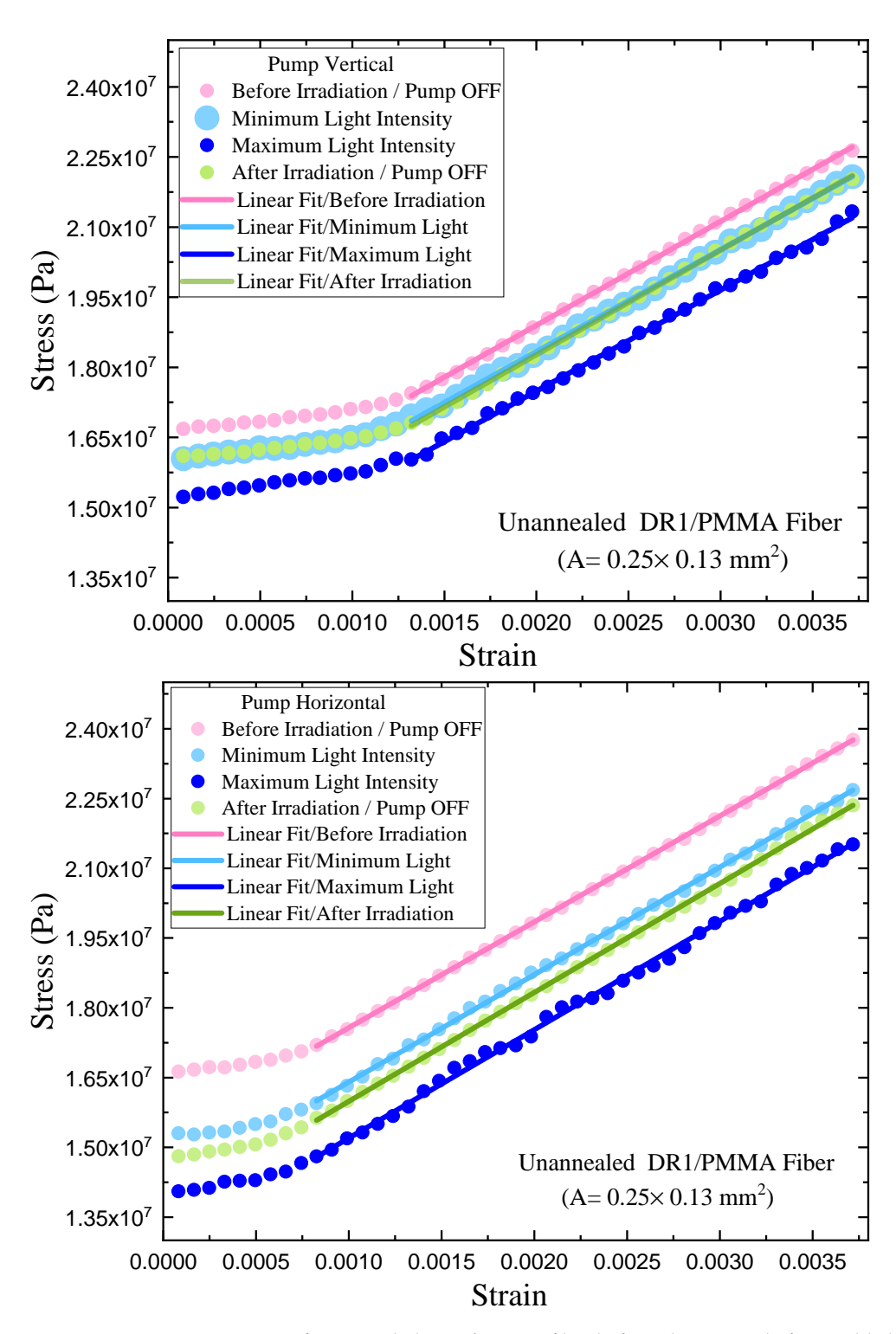


**Figure 9.** Stress versus Strain of unannealed DR1/PMMA fiber before, during, and after visible light irradiation with vertical and horizontal polarization.

Stress versus strain curves are used to determine Young's modulus as a function of absorbed pump intensity for both vertical and horizontal polarization in both plain and dyedoped fibers. Figures 11 and 12 show that for both fibers, Young's modulus is constant before, during, and after irradiation and is not polarization dependent. So, while there is an offset in the strain induced by light, it does not affect the slope of the stress versus strain curve.

Appl. Sci. 2022, 12, 7991 16 of 26

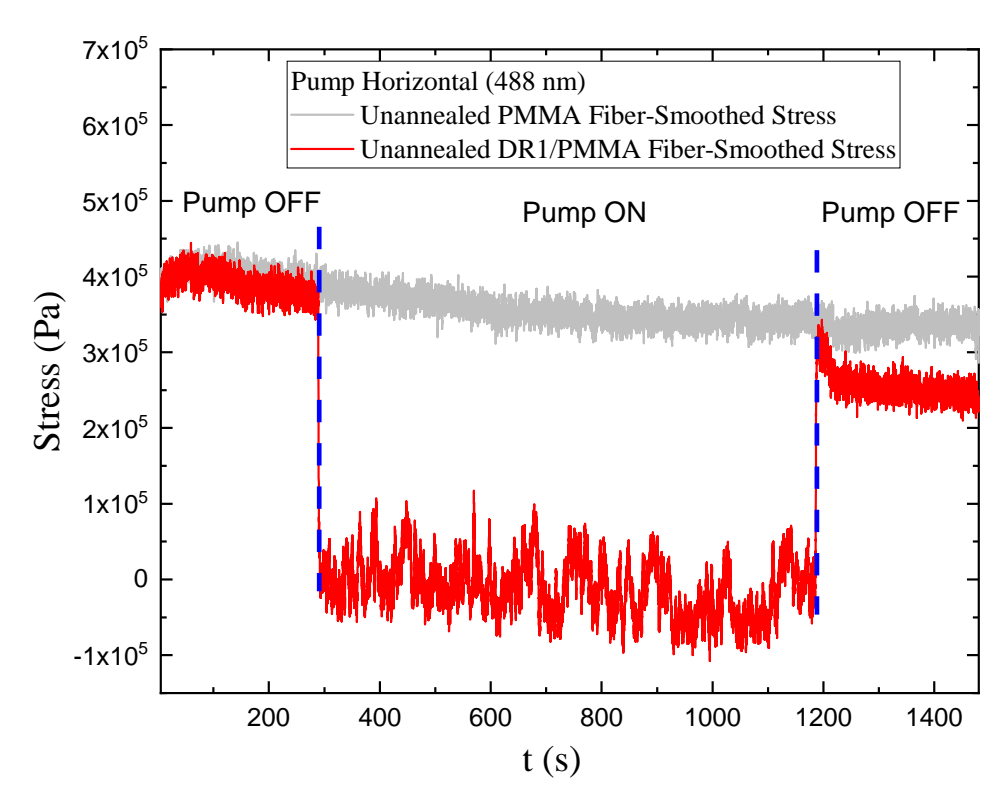


**Figure 10.** Stress as a function of time for unannealed PMMA and DR1/PMMA fibers when the pump is on and off.

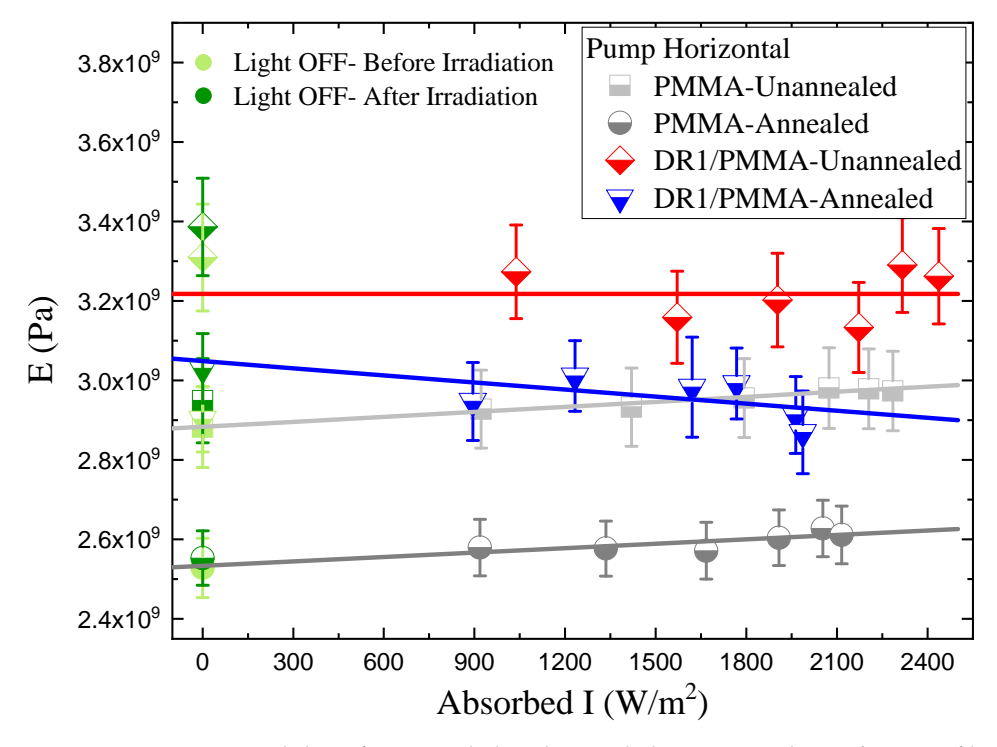


**Figure 11.** Young's Modulus of unannealed and annealed PMMA and DR1/PMMA fibers as a function of horizontally polarized absorbed pump intensity. The lines are fits to the non-zero-intensity data points.

Appl. Sci. **2022**, 12, 7991 17 of 26

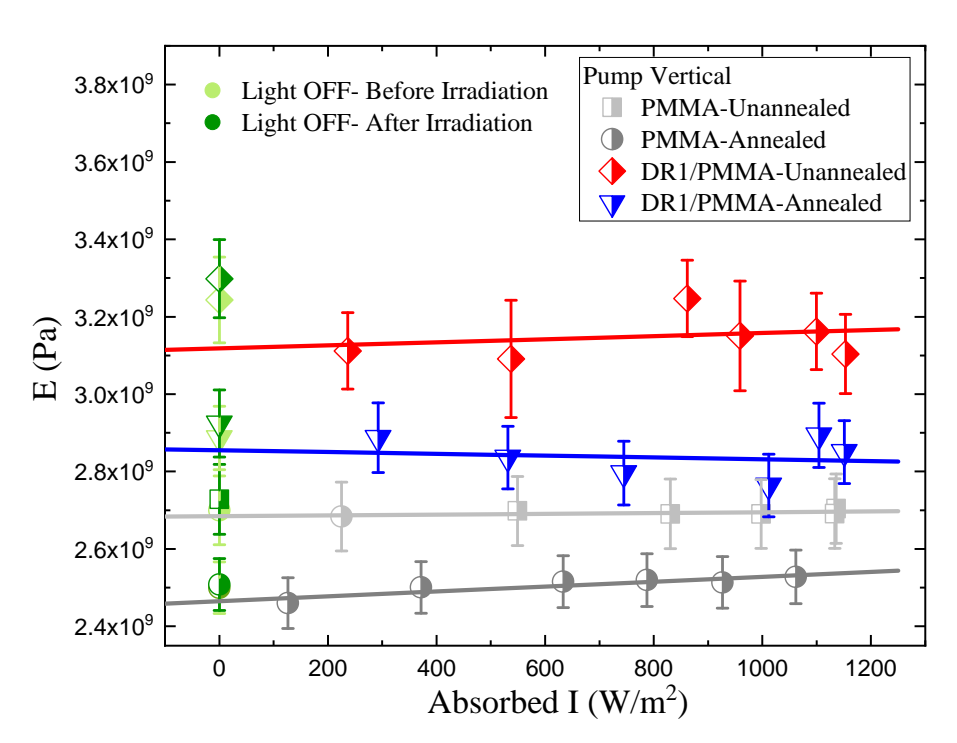


**Figure 12.** Young's Modulus of unannealed and annealed PMMA and DR1/PMMA fibers as a function of vertically polarized absorbed pump intensity. The lines are fits to the non-zero-intensity data points.

Next, we illuminate each sample with maximum light intensity for almost an hour and its Young's modulus is measured before, during, and after illumination with both polarizations of light. Figures 13 and 14 show that visible light does not induce any permanent changes to the Young's modulus of all the fibers for both polarizations. Since PMMA is transparent in the visible range, no change in its Young's modulus is expected. It was shown that the elastic modulus of PMMA thin films remains constant upon irradiation with UV and visible light [48]. Adding an isomerizable dye does not result in a persistent change of Young's modulus after visible irradiation, but it does induce a persistent and transient stress.

The photomechanical effect in DR1/PMMA fibers is known to be reversible; so, it restores the stress to its initial value [16]. In contrast, a DR1/PMMA film in which the DR1 dye is grafted as a side chain pendent shows a persistent decrease in the elastic modulus after irradiating the sample with 487-nm light [33]. In addition, azobenzene-containing films showed that upon visible irradiation the elastic modulus can increase or decrease [49–52]. These differences can be due to differences in azobenzene molecules used, sample preparation methods, sample geometry, wavelength, the polarization of the pump light, and the experimental protocols.

To measure the contribution of photothermal heating to the photomechanical stress response, the PMMA fibers are painted with black markers that absorb all of the light, converting all of the energy to heat. These fibers are irradiated with 488 nm-wavelength light and the stress response as a function of time is measured for vertically and horizontally polarized pump light. Figure 15 shows typical data for the stress versus time for one full cycle of painted fiber. The black points are the smoothed data and the solid curve is a fit to a single exponential. The fit is based on the model developed previously [16,23], given by

$$\sigma_{\rm on} = \sigma^{(0)} + \sigma^{(1)} (1 - e^{(-t/t_1)}) \tag{16}$$

and

$$\sigma_{\text{off}} = \sigma^{(0)} + \sigma^{(1)} (1 - e^{(-t_0/t_1)}) e^{-(t-t_0)/t_2}, \tag{17}$$

Appl. Sci. 2022, 12, 7991 18 of 26

where  $\sigma^{(n)}$ ,  $t_1$ , and  $t_2$  are the amplitudes, turn-on time constant when the pump is on, and turn-off time constant when the pump is off, respectively.  $t_0 = 30 \,\mathrm{s}$  is the time duration of the beam being on and off.

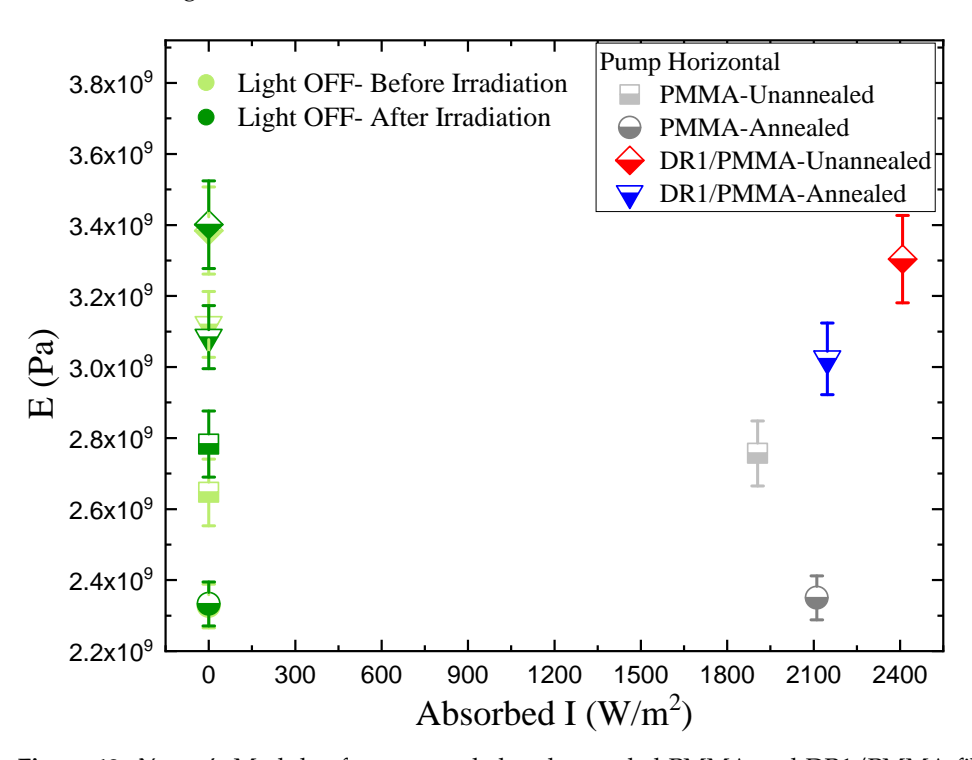


**Figure 13.** Young's Modulus for unannealed and annealed PMMA and DR1/PMMA fibers as a function of maximum horizontally polarized absorbed pump intensity.

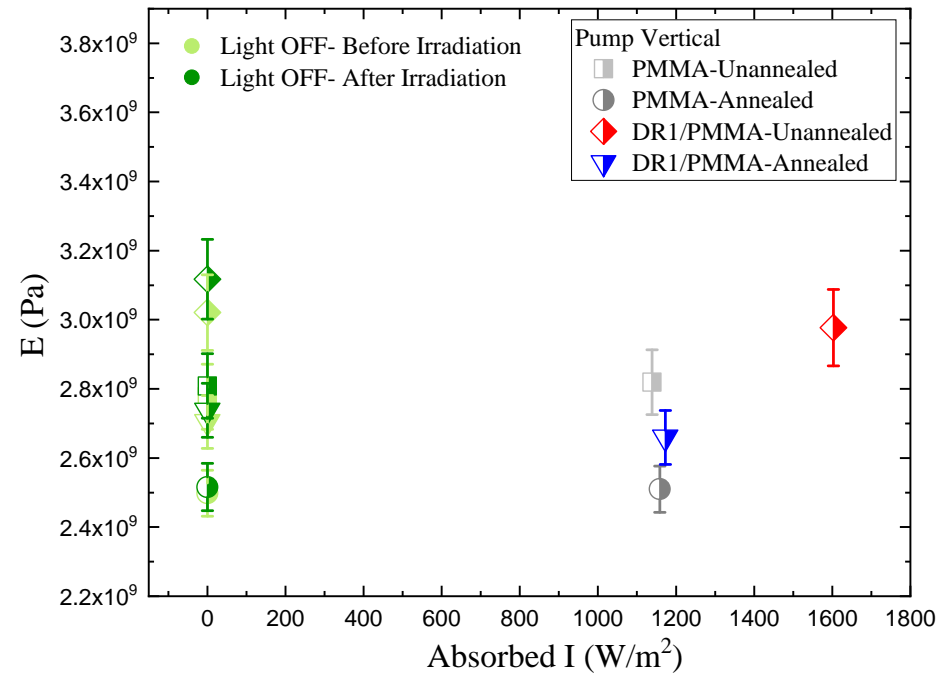


**Figure 14.** Young's Modulus for unannealed and annealed PMMA and DR1/PMMA fibers as a function of maximum vertically polarized absorbed pump intensity.

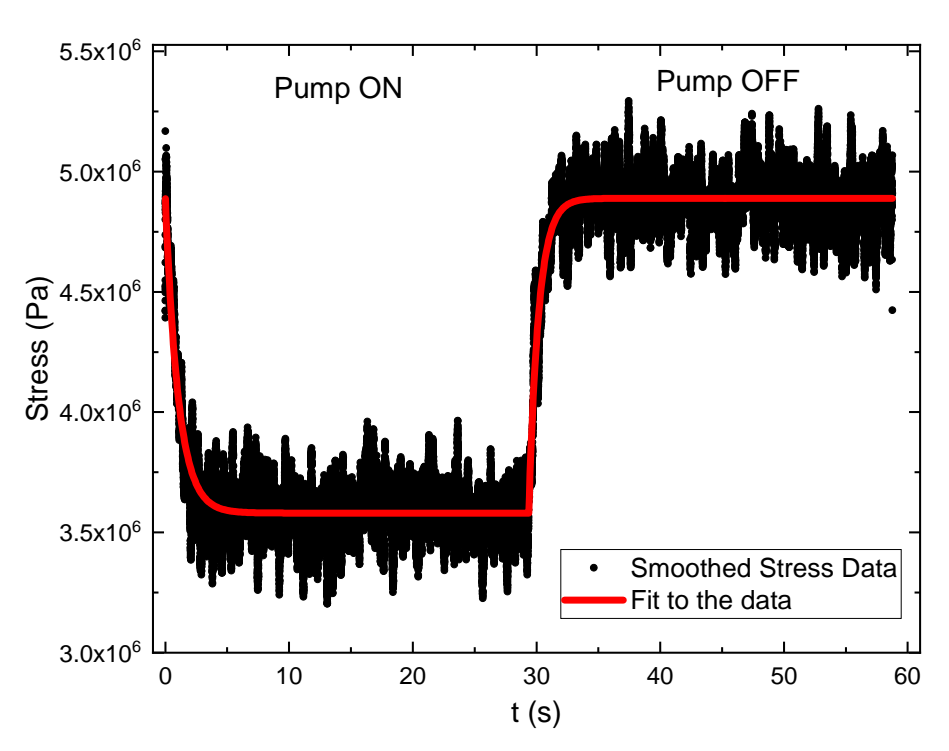


**Figure 15.** Typical smoothed stress versus time data and a fit to Equations (16) and (17) for one full On/OFF cycle.

 $\sigma^{(1)}$  represents the strength of the photomechanical stress response of the material. This stress, when divided by the intensity of the light I that induces this stress, is the definition of the photomechanical constant. Details of this definition can be found in the literature [16,22].

If the sole mechanism is photothermal heating, as it should be in such painted fibers, then  $t_1$  and  $t_2$  should be the same as the Newton heating and cooling time constants [23]. Figures 16 and 17 show the turn-on and turn-off time constants  $t_1$  and  $t_2$  as a function of intensity that are derived using the fitting functions in Equations (16) and (17). We will assume that these are the Newton heating/cooling time constants to determine the photothermal heating contribution.

The photothermal heating contribution to the photomechanical response can be determined from Equation (7).  $\Delta T/I_0$  is determined using Equation (5). Table 4 lists the independently determined values of  $\rho$  and c for PMMA and w is measured with a caliper for the fiber used in our measurements.  $d\sigma/dT$  is calculated from the values in Table 5, which are determined from fits to the temperature-dependent stress as described above. The heating contribution to the photomechanical response are shown in Figure 18. "|" and "—" denote the response along and perpendicular to the long axis of the fibers, which are mounted vertically [23].

The photomechanical response for PMMA fibers marked with black ink and DR1/PMMA fibers as a function of temperature cluster at about  $\kappa_{\sigma}^{(1)}=400~\text{s/m}$  for both polarizations as well as for the painted and unpainted fibers. The response in painted PMMA fibers is only due to heating. The fact that this is the same as the response in unpainted DR1/PMMA fibers strongly suggests that the contribution of photoisomerization and/or molecular reorientation in DR1/PMMA fibers to the photomechanical response is negligible. Furthermore, the fact that the time constants of the response for both painted and unpainted fibers are the same also suggests that the heating mechanism dominates.

Appl. Sci. 2022, 12, 7991 20 of 26

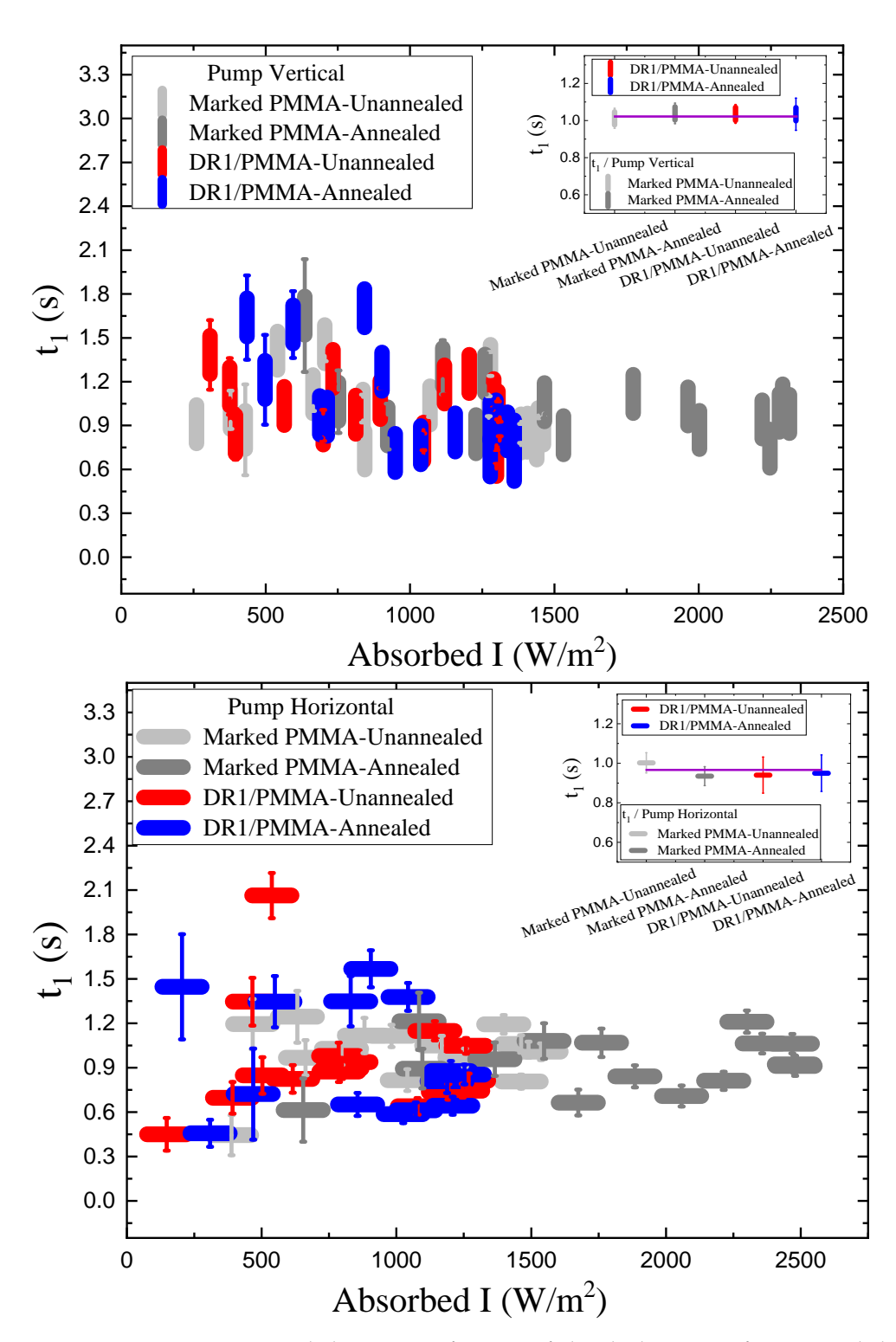


**Figure 16.** Time constant  $t_1$ —light on—as a function of absorbed intensity for unannealed and annealed PMMA and DR1/PMMA fibers for vertical and horizontal pump polarization. The insets show the average time constants over all intensities as a function of the fiber's composition. The "marked" samples are those whose surfaces are painted black to prevent light from entering that sample, resulting in surface heating only.

Appl. Sci. 2022, 12, 7991 21 of 26

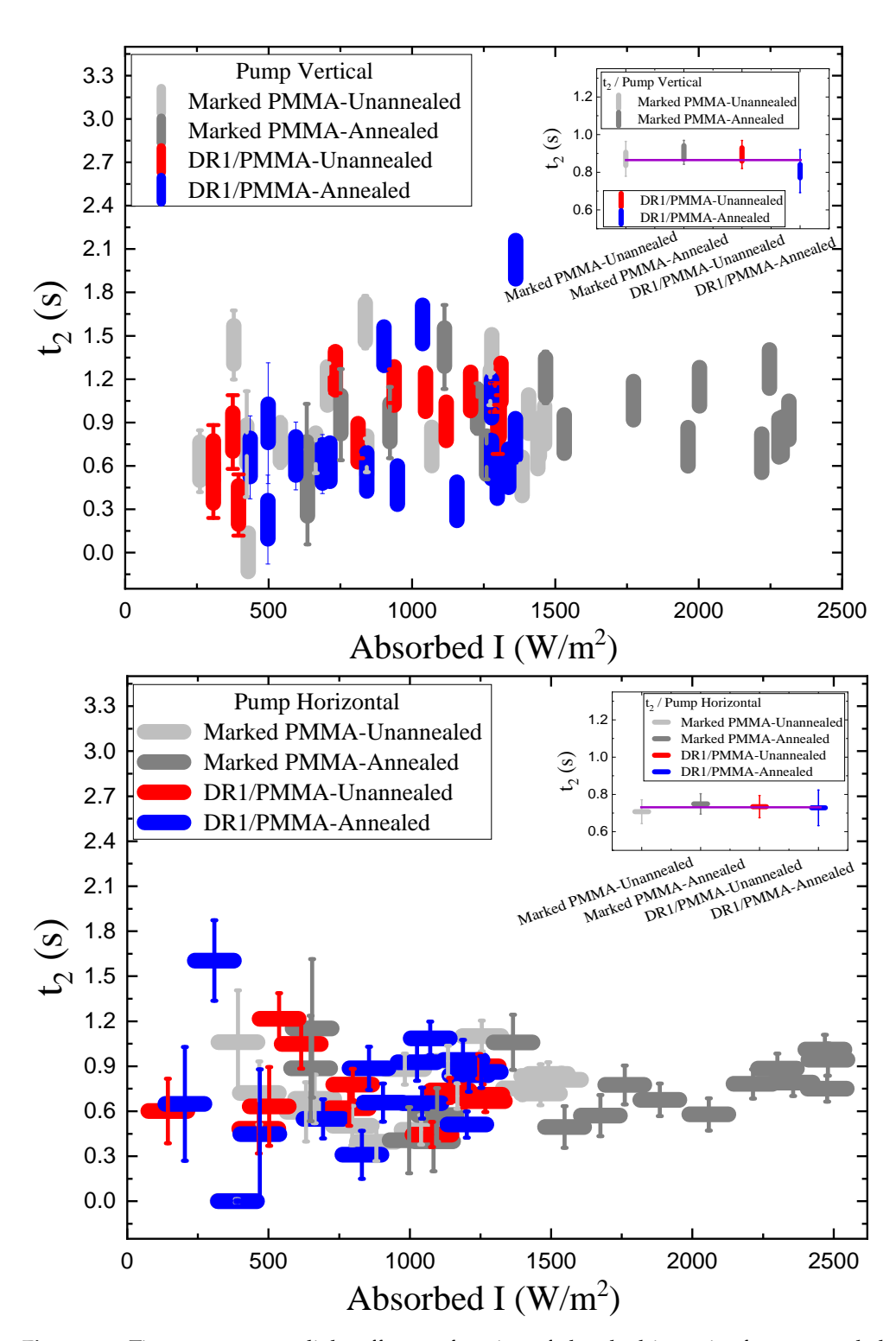


**Figure 17.** Time constant  $t_2$ —light off—as a function of absorbed intensity for unannealed and annealed PMMA and DR1/PMMA fibers for vertical and horizontal pump polarization. The insets show the average time constants over all intensities as a function of the fiber's composition. The "marked" samples are those whose surfaces are painted black to prevent light from entering that sample, resulting in surface heating only.

Appl. Sci. **2022**, 12, 7991 22 of 26

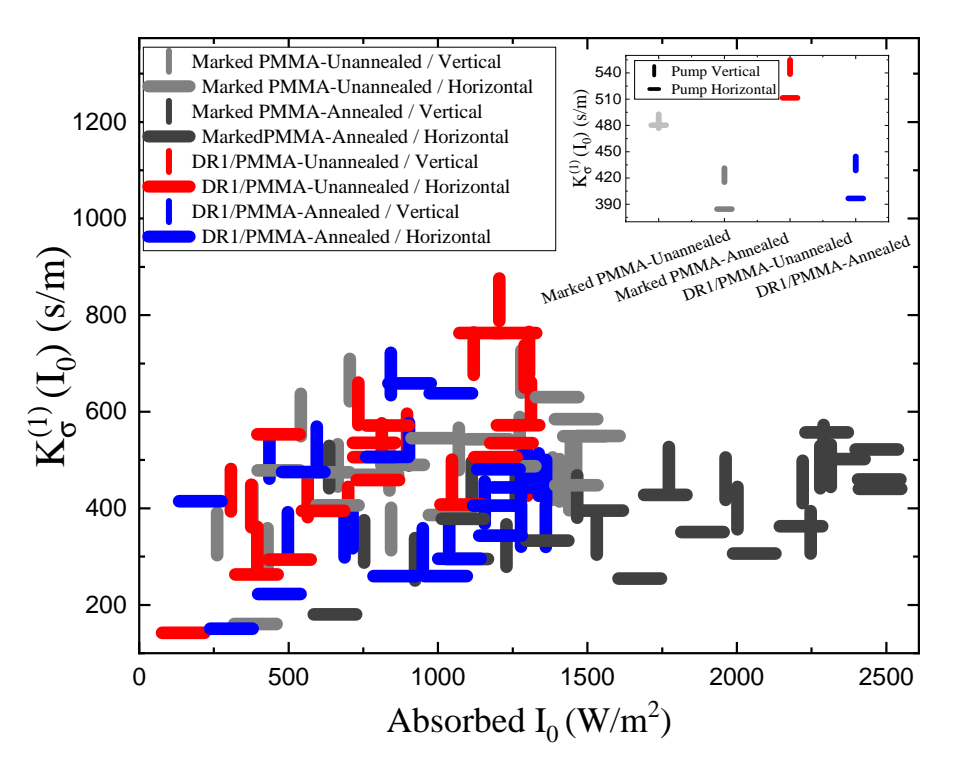


**Figure 18.** The photothermal heating contribution to the photomechanical response as a function of the static absorbed intensity  $I_0$  derived using Equation (7). The "marked" fibers are painted with black marker ink. The inset shows the contribution of each fiber averaged over all intensities.

**Table 4.** Density  $\rho$ , the specific heat c, and thickness w of the fibers used in the models in this paper are from the literature [23,41].

Sample	$\rho$ (kg/m <sup>3</sup> )	c (J/kg K)	w (mm)
PMMA-Unannealed	$1.19 \times 10^{3}$	$1.42 \times 10^{3}$	0.14
PMMA-Annealed	$1.19 \times 10^{3}$	$1.42 \times 10^{3}$	0.15
DR1/PMMA-Unannealed	$1.19 \times 10^{3}$	$1.42 \times 10^{3}$	0.13
DR1/PMMA-Annealed	$1.19 \times 10^{3}$	$1.42\times10^3$	0.14

**Table 5.** The parameters determined from fitting the temperature-dependent stress data in Figure 6 to Equation (6).

Sample	$\sigma_0$ (MPa)	$\sigma_1$ (MPa)	<i>T</i> <sub>0</sub> (K)	п
PMMA-Unannealed	$-10 \ (\pm 0)$	$12.25~(\pm 0.01)$	$327.02 \ (\pm 0.04)$	$13.99 (\pm 0.04)$
PMMA-Annealed	$-10 \ (\pm 0)$	11.86 (±0.01)	330.64 (±0.03)	14.29 (±0.04)
DR1/PMMA- Unannealed	$-10 \ (\pm 0)$	11.21 ( $\pm 0.01$ )	327.91 (±0.01)	$18.80\ (\pm0.04)$
DR1/PMMA- Annealed	$-10 \ (\pm 0)$	11.36 (±0.01)	331.16 (±0.02)	15.83 (±0.04)

The inset of Figure 7 shows the photomechanical response for the dye-doped fiber and the painted plain PMMA fiber, unannealed and annealed. There are several important features of the data. First, in all of the fibers, the thermal contribution to the photomechanical response is approximately independent of the polarization of the pump beam. The difference between the two polarizations for each fiber is at most about  $\pm 5\%$  from the mean. As such, the largest contribution from other mechanisms is bounded by  $\pm 5\%$ . Secondly, the photothermal response is smaller when the fibers are annealed. This could be due to

Appl. Sci. **2022**, 12, 7991 23 of 26

the fact that after annealing, the internal stress that adds to the photomechanical response has been released. Further, the photomechanical response for pump beam polarization perpendicular to the strain direction is consistently lower than for the parallel polarization. This effect, though small, could be from the broken symmetry by the uniaxial strain direction. Finally, we find the plain PMMA fibers that are marked with ink have the same photomechanical response as the dye-doped ones when comparing the unannealed ones as well as the annealed ones.

The temperature-dependent figure of merit is also measured to determine if elevated temperature can increase their efficiencies. It is derived using Equation (11) and is shown in Figure 19. The result shows that increasing temperature increases the figure of merit and indicates that controlling the temperature can improve the response of such materials. The largest change is for unannealed DR1-doped PMMA, which shows a linear dependence with a slope of  $10\% \text{ K}^{-1}$ —a dramatic increase.

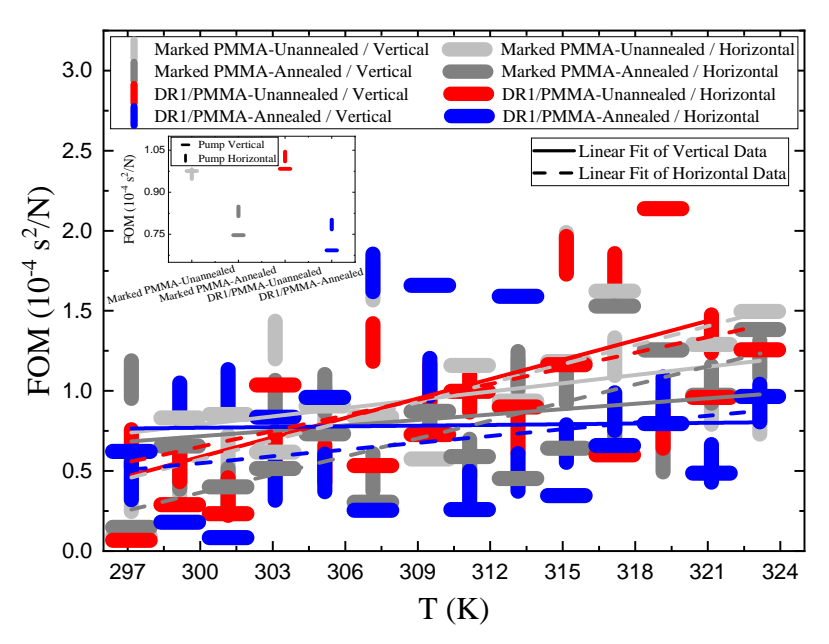


**Figure 19.** Figure of merit as a function of temperature for PMMA and DR1/PMMA fibers derived using Equation (11). The inset shows the average FOM over all intensities as a function of fiber composition and processing. The lines are fits to each composition and processing condition.

#### 5. Conclusions

We have investigated the effect of adding dye and annealing on the thermomechanical and photomechanical properties of PMMA fibers by measuring the intensity-, polarization-, and temperature-dependent Young's modulus and stress. The results show that adding DR1 to PMMA leads to antiplasticization by increasing the stiffness and lowering the  $T_g$  in the fiber geometry. Moreover, annealing the fibers at 90 °C for several days decreases their stiffness and increases their  $T_g$  since it reduces chain alignment and, thereby, increases entropy. The change in stress in DR1-doped PMMA fibers is greater than in plain ones because of their lower  $T_g$ , which leads to a more facile rearrangement of the polymer chains.

The fibers' stiffness is not affected by light illumination at a wavelength of 488 nm, independent of polarization, but the absolute stress changes in response to light. The process is found to be reversible, returning the stress to its original value after the pump light is turned off.

Models are proposed to fit the temperature-dependent Young's modulus and stress. The data fit the models well and are used to determine the critical temperatures, which, in annealed fibers, is greater than in unannealed ones. This observation is consistent with the decrease in  $T_g$  upon annealing and adding a dopant dye.

Appl. Sci. 2022, 12, 7991 24 of 26

A comparison of dye-doped fibers with plain fibers is used as a control. We find that the dominant photomechanical mechanism in DR1/PMMA is photothermal heating. The time response derived using stress versus time data fits a single exponential, which suggests that only one mechanism is involved.

The measured temperature-dependence of Young's modulus and the photomechanical constant are used to determine the temperature-dependent figure of merit, which defines the efficiency of a material in converting light energy to mechanical work. The results show that increasing the temperature increases the FOM and suggest that higher temperatures are desirable for having more efficient photomechanical materials.

This set of results suggest ways in which the thermomechanical and photomechanical properties of a dye-doped polymer can be controlled to optimize it for a particular application. The techniques introduced here can also be used to study the physics of the photomechanical response and how it is affected by the rheological properties of the material.

**Author Contributions:** Conceptualization, M.G.K.; methodology, M.G.K.; software, B.Z.; validation, B.Z., Z.G. and M.S.K.; formal analysis, M.G.K. and Z.G.; investigation, Z.G., M.S.K., M.G.K., B.Z. and R.O.; resources, M.G.K.; data curation, B.Z., Z.G. and M.G.K.; writing—original draft preparation, Z.G. and M.G.K.; writing—review and editing, M.G.K., Z.G., B.Z., R.O. and M.S.K.; visualization, Z.G. and M.G.K.; supervision, M.G.K.; project administration, M.G.K.; funding acquisition, M.G.K. All authors have read and agreed to the published version of the manuscript.

**Funding:** This research was funded by The National Science Foundation, Directorate for Engineering (ENG) grant number EFRI-ODISSEI:1332271.

Institutional Review Board Statement: Not applicable.

**Informed Consent Statement:** Not applicable.

**Data Availability Statement:** https://www.dropbox.com/sh/oxoexzdunuqd7is/AADaFOAvHu\_6ddjn16erigIra?dl=0 (accessed on 7 August 2022).

**Acknowledgments:** The authors thank the National Science Foundation (EFRI-ODISSEI:1332271) for supporting this work.

**Conflicts of Interest:** The authors declare no conflict of interest.

Sample Availability: Samples of the compounds are available from Z.G., M.S.K., or R.O.

# **Abbreviations**

The following abbreviations are used in this manuscript:

DR1 Disperse Red 1

PMMA Poly(methyl methacrylate)  $T_g$  Glass Transition Temperature

POF Polymer Optical Fiber FOM Figure of Merit MMA Methyl Methacrylate

INT Initiator

CTA Chain Transfer Agent

# References

- 1. Xiong, Z.; Peng, G.D.; Chu, P.L. Nonlinear coupling and optical switching in a beta-carotene-doped twin-core polymer optical fiber. *Opt. Eng.* **2000**, 39, 624–627. [CrossRef]
- 2. Jiang, C.; Kuzyk, M.G.; Ding, J.L.; Johns, W.E.; Welker, D.J. Fabrication and mechanical behavior of dye-doped polymer optical fiber. *J. Appl. Phys.* **2002**, 92, 4–12. [CrossRef]
- 3. Aitchison, J.S.; Villeneuve, A.; Stegeman, G.I. All-optical switching in two cascaded nonlinear directional couplers. *Opt. Lett.* **1995**, 20, 698. [CrossRef]
- 4. Asobe, M.; Naganuma, K.; Kaino, T.; Kanamori, T.; Tomaru, S.; Kurihara, T. Switching energy limitation in all-optical switching due to group velocity dispersion of highly nonlinear optical waveguides. *Appl. Phys. Lett.* **1994**, *64*, 2922–2924. [CrossRef]
- 5. Assanto, G.; Stegeman, G.; Sheik-Bahae, M.; Stryland, E.V. All-optical switching devices based on large nonlinear phase shifts from second harmonic generation. *Appl. Phys. Lett.* **1993**, *62*, 1323–1325. [CrossRef]

Appl. Sci. **2022**, 12, 7991 25 of 26

6. Eggleton, B.J.; Slusher, R.E.; Judkins, J.B.; Stark, J.B.; Vengsarkar, A.M. All-optical switching in long-period fiber gratings. *Opt. Lett.* **1997**, 22, 883. [CrossRef]

- 7. Fork, R. Physics of optical switching. *Phys. Rev. A* 1982, 26, 2049. [CrossRef]
- 8. He, G.S.; Zhu, J.; Baev, A.; Samoć, M.; Frattarelli, D.L.; Watanabe, N.; Facchetti, A.; Ågren, H.; Marks, T.J.; Prasad, P.N. Twisted π-System Chromophores for All-Optical Switching. *J. Am. Chem. Soc.* **2011**, *133*, 6675–6680. [CrossRef]
- 9. Jinno, M.; Matsumoto, T. Ultrafast, Low Power, and Highly Stable All-Optical Switching inan All Polarization Maintaining Fiber Sagnac Interferometer. *IEEE Photonics Technol. Lett.* **1990**, 2, 349. [CrossRef]
- Welker, D.J.; Kuzyk, M.G. All-optical switching in a dye-doped polymer fiber Fabry–Perot waveguide. Appl. Phys. Lett. 1996, 69, 1835–1836. [CrossRef]
- 11. Tagaya, A.; Koike, Y.; Kinoshita, T.; Nihei, E.; Yamamoto, T.; Sasaki, K. Polymer optical fiber amplifier. *Appl. Phys. Lett.* **1993**, 63, 883–884. [CrossRef]
- 12. Koynov, K.; Saltiel, S.; Buchvarov, I. All-optical switching by means of an interferometer with nonlinear frequency doubling mirrors. *J. Opt. Soc. Am. B* **1997**, *14*, 834. [CrossRef]
- 13. Silberberg, Y.; Perimutter, P.; Baran, J.E. Digital Optical Switch. Appl. Phys. Lett. 1987, 51, 1230–1232. [CrossRef]
- 14. Ono, M.; Hata, M.; Tsunekawa, M.; Nozaki, K.; Sumikura, H.; Chiba, H.; Notomi, M. Ultrafast and energy-efficient all-optical switching with graphene-loaded deep-subwavelength plasmonic waveguides. *Nat. Photonics* **2019**, *14*, 37–43. [CrossRef]
- 15. Li, Y.; Bhattacharyya, A.; Thomidis, C.; Moustakas, T.D.; Paiella, R. Ultrafast all-optical switching with low saturation energy via intersubband transitions in GaN/AlN quantum-well waveguides. *Opt. Express* **2007**, *15*, 17922. [CrossRef]
- 16. Zhou, B.; Bernhardt, E.; Bhuyan, A.; Ghorbanishiadeh, Z.; Rasmussen, N.; Lanska, J.; Kuzyk, M.G. Theoretical and experimental studies of photomechanical materials [Invited]. *J. Opt. Soc. Am. B* **2019**, *36*, 1492. [CrossRef]
- 17. Kuzyk, M.G.; Garvey, D.W.; Canfield, B.K.; Vigil, S.R.; Welker, D.J.; Tostenrude, J.; Breckon, C. Characterization of single-mode polymer optical fiber and electrooptic fiber devices. *Chem. Phys.* **1999**, 245, 327–340. [CrossRef]
- 18. Ishiyama, C.; Higo, Y. Effects of humidity on Young's modulus in poly(methyl methacrylate). *J. Polym. Sci. Part B Polym. Phys.* **2002**, *40*, 460–465. [CrossRef]
- 19. Hamouda, A.M.S. The influence of humidity on the deformation and fracture behaviour of PMMA. *J. Mater. Process. Technol.* **2002**, 124, 238–243. [CrossRef]
- 20. Kuzyk, M.G.; Paek, U.C.; Dirk, C.W. Guest-host polymer fibers for nonlinear optics. Appl. Phys. Lett. 1991, 59, 902–904. [CrossRef]
- 21. Mahimwalla, Z.; Yager, K.G.; Ichi Mamiya, J.; Shishido, A.; Priimagi, A.; Barrett, C.J. Azobenzene photomechanics: Prospects and potential applications. *Polym. Bull.* **2012**, *69*, 967–1006. [CrossRef]
- 22. Kuzyk, M.G.; Dawson, N.J. Photomechanical materials and applications: A tutorial. Adv. Opt. Photonics 2020, 12, 847. [CrossRef]
- 23. Ghorbanishiadeh, Z.; Zhou, B.; Karkhaneh, M.S.; Oehler, R.; Kuzyk, M.G. Photothermal and Reorientational Contributions to the Photomechanical Response of DR1 Azo Dye-Doped PMMA Fibers. *Appl. Sci.* **2021**, *12*, 315. [CrossRef]
- 24. Taniguchi, T.; Asahi, T.; Koshima, H. Photomechanical Azobenzene Crystals. Crystals 2019, 9, 437. [CrossRef]
- 25. Riggleman, R.A.; de Pablo, J.J. Antiplasticization and local elastic constants in trehalose and glycerol mixtures. *J. Chem. Phys.* **2008**, *128*, 224504. [CrossRef] [PubMed]
- 26. Delcambre, S.P.; Riggleman, R.A.; de Pablo, J.J.; Nealey, P.F. Mechanical properties of antiplasticized polymer nanostructures. *Soft Matter* **2010**, *6*, 2475. [CrossRef]
- 27. Riggleman, R.A.; Douglas, J.F.; de Pablo, J.J. Antiplasticization and the elastic properties of glass-forming polymer liquids. *Soft Matter* **2010**, *6*, 292–304. [CrossRef]
- 28. Mascia, L.; Kouparitsas, Y.; Nocita, D.; Bao, X. Antiplasticization of Polymer Materials: Structural Aspects and Effects on Mechanical and Diffusion-Controlled Properties. *Polymers* **2020**, *12*, 769. [CrossRef]
- 29. Soong, S.Y.; Cohen, R.E.; Boyce, M.C.; Chen, W. The effects of thermomechanical history and strain rate on antiplasticization of PVC. *Polymer* **2008**, *49*, 1440–1443. [CrossRef]
- 30. Lei, D.; Runt, J.; Safari, A.; Newnham, R.E. Dielectric properties of azo dye-poly(methyl methacrylate) mixtures. *Macromolecules* **1987**, 20, 1797–1801. [CrossRef]
- 31. Abdel-Wahab, A.A.; Ataya, S.; Silberschmidt, V.V. Temperature-dependent mechanical behaviour of PMMA: Experimental analysis and modelling. *Polym. Test.* **2017**, *58*, 86–95. [CrossRef]
- 32. Amalia, N.; Yuliza, E.; Margaretta, D.O.; Utami, F.D.; Surtiyeni, N.; Viridi, S.; Abdullah, M. A novel method for characterizing temperature-dependent elastic modulus and glass transition temperature by processing the images of bending cantilever slender beams at different temperatures. *AIP Adv.* **2018**, *8*, 115201. [CrossRef]
- 33. Sorelli, L.; Fabbri, F.; Frech-Baronet, J.; Vu, A.D.; Fafard, M.; Gacoin, T.; Lahlil, K.; Martinelli, L.; Lassailly, Y.; Peretti, J. A closer look at the light-induced changes in the mechanical properties of azobenzene-containing polymers by statistical nanoindentation. *J. Mater. Chem. C* 2015, *3*, 11055–11065. [CrossRef]
- 34. Sekkat, Z.; Wood, J.; Knoll, W. Reorientation Mechanism of Azobenzenes within the Trans ⇒ Cis Photoisomerization. *J. Phys. Chem.* **1995**, *99*, 17226–17234. [CrossRef]
- 35. Sekkat, Z.; Yasumatsu, D.; Kawata, S. Pure Photoorientation of Azo Dye in Polyurethanes and Quantification of Orientation of Spectrally Overlapping Isomers. *J. Phys. Chem. B* **2002**, *106*, 12407–12417. [CrossRef]
- 36. Sekkat, Z. Vectorial motion of matter induced by light fueled molecular machines. OSA Contin. 2018, 1, 668. [CrossRef]

Appl. Sci. **2022**, 12, 7991 26 of 26

37. Naumov, P.; Chizhik, S.; Panda, M.K.; Nath, N.K.; Boldyreva, E. Mechanically Responsive Molecular Crystals. *Chem. Rev.* **2015**, 115, 12440–12490. [CrossRef]

- 38. Chizhik, S.; Sidelnikov, A.; Zakharov, B.; Naumov, P.; Boldyreva, E. Quantification of photoinduced bending of dynamic molecular crystals: From macroscopic strain to kinetic constants and activation energies. *Chem. Sci.* **2018**, *9*, 2319–2335. [CrossRef]
- 39. Taniguchi, T.; Blanc, L.; Asahi, T.; Koshima, H.; Lambert, P. Statistical Modeling of Photo-Bending Actuation of Hybrid Silicones Mixed with Azobenzene Powder. *Actuators* **2019**, *8*, 68. [CrossRef]
- 40. Megson, T.H.G. Structural and Stress Analysis, 2nd ed.; Butterworth-Heinemann: Oxford, UK, 2005.
- 41. Kuzyk, M.G.; Dirk, C.W.; Sohn, J.E. Mechanisms of quadratic electro-optic modulation of dye-doped polymer systems. *J. Opt. Soc. Am. B* **1990**, *7*, 842. [CrossRef]
- 42. Bian, S.; Robinson, D.; Kuzyk, M.G. Optically activated cantilever using photomechanical effects in dye-doped polymer fibers. *J. Opt. Soc. Am. B* **2006**, 23, 697. [CrossRef]
- 43. Kuzyk, M.G. Polymer Fiber Optics: Materials, Physics, and Applications; CRC Press: Boca Raton, FL, USA, 2006.
- 44. Harvey, C.L.M.; Terentjev, E.M. Role of polarization and alignment in photoactuation of nematic elastomers. *Eur. Phys. J. E* **2007**, 23, 185–189. [CrossRef] [PubMed]
- 45. Bernhardt, E.A.; Garrison, C.M.; Rasmussen, N.F.; Lanska, J.T.; Kuzyk, M.G. An apparatus for measuring a material's photomechanical response. *Am. J. Phys.* **2018**, *86*, 943–952. [CrossRef]
- 46. Dawson, N.J.; Kuzyk, M.G.; Neal, J.; Luchette, P.; Palffy-Muhoray, P. Experimental studies of the mechanisms of photomechanical effects in a nematic liquid crystal elastomer. *J. Opt. Soc. Am. B* **2011**, *28*, 1916. [CrossRef]
- 47. Dawson, N.J.; Kuzyk, M.G.; Neal, J.; Luchette, P.; Palffy-Muhoray, P. Modeling the mechanisms of the photomechanical response of a nematic liquid crystal elastomer. *J. Opt. Soc. Am. B* **2011**, *28*, 2134. [CrossRef]
- 48. Moniruzzaman, M.; Zioupos, P.; Fernando, G.F. Investigation of reversible photo-mechanical properties of azobenzene-based polymer films by nanoindentation. *Scr. Mater.* **2006**, *54*, 257–261. [CrossRef]
- 49. Karageorgiev, P.; Neher, D.; Schulz, B.; Stiller, B.; Pietsch, U.; Giersig, M.; Brehmer, L. From anisotropic photo-fluidity towards nanomanipulation in the optical near-field. *Nat. Mater.* **2005**, *4*, 699–703. [CrossRef]
- 50. Vapaavuori, J.; Mahimwalla, Z.; Chromik, R.R.; Kaivola, M.; Priimagi, A.; Barrett, C.J. Nanoindentation study of light-induced softening of supramolecular and covalently functionalized azo polymers. *J. Mater. Chem. C* **2013**, *1*, 2806. [CrossRef]
- 51. Harrison, J.M.; Goldbaum, D.; Corkery, T.C.; Barrett, C.J.; Chromik, R.R. Nanoindentation studies to separate thermal and optical effects in photo-softening of azo polymers. *J. Mater. Chem. C* **2015**, *3*, 995–1003. [CrossRef]
- 52. Richter, A.; Nowicki, M.; Wolf, B. A Nanoindentation Study of Photo-Induced Changes in Polymers Containing Azobenzene. Mol. Cryst. Liq. Cryst. 2008, 483, 49–61. [CrossRef]